

Novel 1-Hydroxypiperazine-2,6-diones as New Leads in the Inhibition of Metalloproteinases

Sérgio M. Marques,[†] Tiziano Tuccinardi,^{*,‡} Elisa Nuti,[‡] Salvatore Santamaria,^{‡,§} Vânia André,[†] Armando Rossello,[‡] Adriano Martinelli,[‡] and M. Amélia Santos^{*,†}

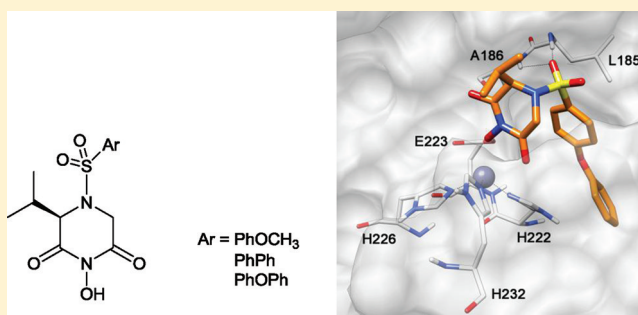
[†]Centro de Química Estrutural, Instituto Superior Técnico, Av. Rovisco Pais 1, 1049-001 Lisboa, Portugal

[‡]Dipartimento di Scienze Farmaceutiche, Università degli Studi di Pisa, Via Bonanno 6, 56126 Pisa, Italy

[§]Kennedy Institute of Rheumatology Division, Faculty of Medicine, Imperial College London, 65 Aspenlea Road, London W6 8LH, United Kingdom

S Supporting Information

ABSTRACT: New compounds containing a novel zinc-binding group (1-hydroxypiperazine-2,6-dione, HPD) have been identified as effective inhibitors of matrix metalloproteinases (MMPs), with activities in the nanomolar concentration range. That moiety seemed to bind the catalytic zinc ion of MMPs, revealing itself as a new potential substitute for the hydroxamate group in the next generation of metalloproteinase inhibitors. The X-ray crystal structure of **1b** elucidated its 3D conformation and supramolecular packing in solid state. Theoretical procedures were used to investigate the binding mode of this class of compounds, within the active site of MMP13. A computational method involving docking and hybrid quantum mechanical and molecular mechanical (QM/MM) dynamic simulations was developed and applied. This study suggested that the HPD moiety binds bidentately to the catalytic zinc through its oxygen atoms. The final structure obtained will allow straightforward drug design approaches in view of further optimization and development of new MMP inhibitors bearing the HPD moiety.

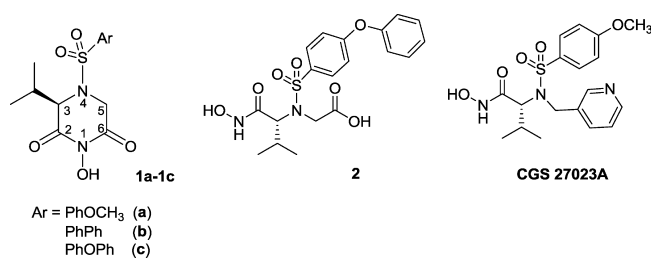


1. INTRODUCTION

Matrix metalloproteinases (MMPs) are a class of zinc-dependent endopeptidases that degrade most components of the extracellular matrix such as collagens and gelatins. These enzymes are normally expressed only in physiological processes of tissue remodeling and repairing, homeostatic regulation, and control of innate immunity. However, in cases of overexpression, they are responsible for several pathological situations involving degradation of the connective tissue, such as rheumatoid arthritis, osteoarthritis, neuroinflammatory diseases, aneurisms, angiogenesis, and tumor invasion.^{1–3} Hence, there has been a demand for synthetic inhibitors that are able to control their activity for the last three decades. Most of the inhibitors reported bear a hydroxamic acid as a zinc-binding group (ZBG) because it provides the strongest inhibitory properties by coordinating the catalytic zinc ion of the MMPs.^{1,4} Except for a few ligands, such as AZD1236, under development by AstraZeneca, and CTS-1027, from Conatus Pharmaceuticals, there are currently no synthetic or biologic MMP inhibitors (MPIs) in clinical trials or in use. This is primarily due to the failure of early studies, which were mainly focused on compounds containing hydroxamate as the zinc-chelating group.^{5,6} A tetracycline derivative, doxycycline (Periostat; CollaGenex Pharmaceuticals Inc., Newtown, PA, USA), is currently the only MPI approved by the U.S. FDA and is used as an adjunct therapy in adult periodontitis.⁷ One of the main reasons for the limitations

of hydroxamate-based inhibitors is due to its poor bioavailability and the toxicity arising from its metabolic stability limitations (the amide bond can be easily hydrolyzed with formation of hydroxylamine and the corresponding carboxylic acids).^{8,9} On the other hand, most of the inhibitors tested were broad-spectrum MMP inhibitors (e.g. CGS 27023A,¹⁰ Chart 1) that make no distinction between these enzymes.

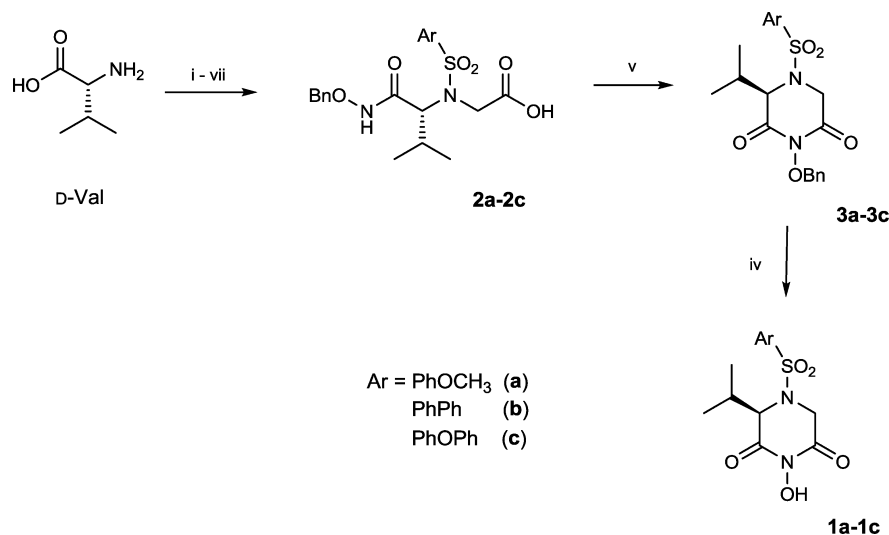
Chart 1



The implication of certain members of the MMP family in cancer and tumor progression is widely accepted, but the difficulty lies in finding the true targets because their roles in the “protease web”

Received: May 12, 2011

Published: October 21, 2011

Scheme 1^a

^aReagents and conditions: (i) ArSO₂Cl, TEA, 1:1 dioxane/H₂O, rt; (ii) BnBr, TEA, CH₃CN, reflux; (iii) BrCH₂COOtBu, K₂CO₃, KI, DMF, rt; (iv) H₂, Pd/C, MeOH, rt; (v) ECF, NMM, THF, 0 °C; (vi) NH₂OBn, MeOH, 0 °C; (vii) TFA, CH₂Cl₂, rt.

are complex. In fact, some MMP members may act as activators of the other enzymes and play important roles in various cascade reactions, which may turn out to be protective against the disease.^{3,8,11,12} Furthermore, concerning the composition and 3D structure of the active site, MMPs are very conservative, which makes it more difficult to develop selective inhibitors. At this point, the type of ZBG in use may be of great importance. Some authors claim that functional groups that chelate the metal ion too strongly may imbalance the importance of the whole of the molecule in binding to the protein, making it difficult to find selectivity for a specific metalloprotein. This may be the case in the hydroxamic group, which forms strong complexes with zinc and other metal ions^{3,4,9,13} and may not only bind indiscriminately to all members of the MMP family but also to other metalloproteinases.¹⁴

The number of drawbacks related to the hydroxamate-based drugs prompted us to investigate new types of ZBGs suitable for use in MMP inhibitors in a tendency followed by others.^{15–17} Such efforts led us to the discovery of a novel ZBG, the 1-hydroxypiperazine-2,6-dione (HPD), which can be successfully included in new inhibitors of MMPs or other metalloproteinases (Chart 1, compounds 1a–c). This group is related to the hydroxamic acids (i.e., compound 2,¹⁸ Chart 1), however, due to its six-membered ring structure, it is expected to be more stable and more resistant to hydrolysis, with additional favorable pharmacokinetic properties. On the other hand, it has previously shown lower binding strength with a series of metal ions, including zinc(II), with respect to the hydroxamic moiety.¹⁹ This discovery drove us to investigate the binding mode of these compounds within MMPs in order to develop new MPis bearing the HPD moiety as ZBG. This group is tractable for structure optimization at three points (3- and 5-positions of the ring and the arylsulfonyl group linked to the 4-position; see Chart 1). This strategy envisages obtaining important enhancements in the activity and selectivity profiles of new inhibitors and thus lead to new effective MMP targeting drugs.

2. CHEMISTRY

The compounds 1a–c appeared as cyclic analogues of previously reported hydroxamic-based compounds such as

compound 2 (Chart 1).¹⁸ Starting from D-valine, 2a–c were prepared after a series of coupling reactions that involved a protection/deprotection strategy with orthogonal activating groups (see Scheme 1, steps i–vii).¹⁸ The reactions of those carboxylic derivatives (2a–c) with a carboxylic-activating agent, through an intramolecular nucleophilic attack of the N-hydroxylamide on the activated carbonyl group, resulted in the 6-ring closure and the formation of compounds 3a–c. The reaction always yielded the same products independently of the activating agent (ECF or TBTU) and the temperature (–40 or 0 °C). This fact clearly indicates that 3a–c are the most thermodynamically stable products of this reaction. After catalytic hydrogenolysis for benzyl deprotection, the target compounds 1a–c were obtained.

To evaluate the aqueous stability of the new compounds, the ¹H NMR spectra were recorded for 1a in D₂O for several days. At pD ca. 2, almost no decomposition was observed for the first 24 h (<1%), only ca. 2% decomposition was observed after 48 h, ca. 5% after 5 days, and ca. 8% after 10 days. At pD ca. 7, almost no decomposition was observed for the first 24 h (<1%), ca. 3% after 3 days, ca. 6% after 5 days, and ca. 7% after 20 days. These results suggest considerable stability of the HPD moiety to hydrolysis both in acidic and neutral conditions.

3. RESULTS AND DISCUSSION

3.1. X-ray Crystallographic Structure of Compound 1b

Single crystals of compound 1b were obtained from the slow evaporation of a solution of pure compound in dichloromethane. The crystalline displayed a monoclinic symmetry, and the acentric P2₁ space group supported the chirality of the molecule. All the distances and angles were within the expected values for related compounds.

The molecules interacted with each other via the (N–)O–H···O(–S) (0.82 Å; 1.90 Å; 2.697(3) Å; 163°) H-bond. Although this was not necessarily the active species, it allowed us to draw conclusions relatively to the correct 3D conformation of the ligand in the molecular modeling structures with MMP13 and to the selection of the proposed binding hypothesis (vide infra).

The supramolecular arrangement of **1b** is characterized by C(8) chains along the *a* axis, which are formed by the above-mentioned interaction (Figure 1B). Furthermore, C–H··· π interactions between

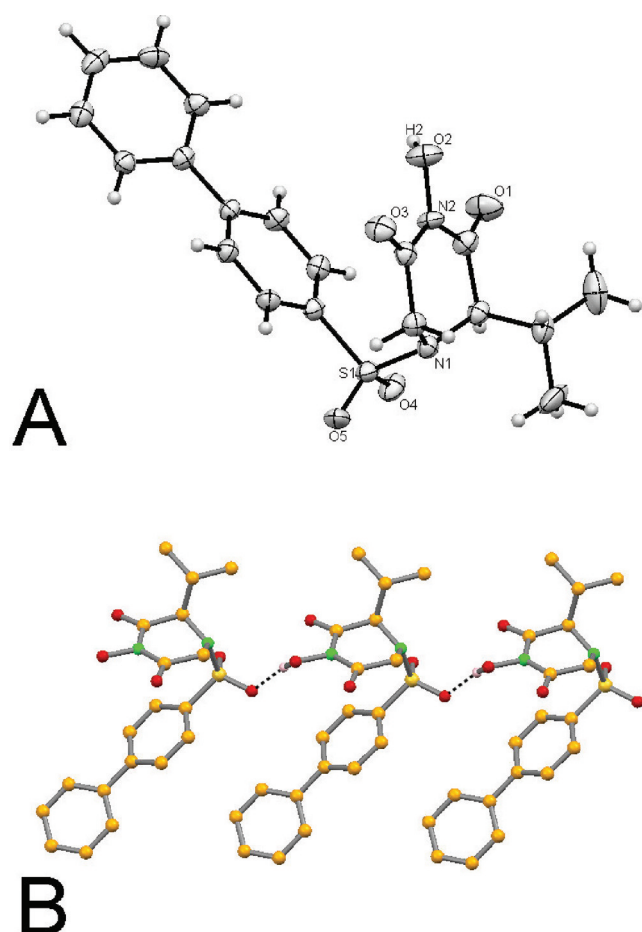


Figure 1. (a) ORTEP diagram for compound **1b** with ellipsoids set at 50%. (b) Supramolecular arrangements of compound **1b** showing the chain formed along *a* via (N–)O–H···O(–S) hydrogen bonds.

the CH₂ of the HPD moiety and the π system terminal ring of the biphenyl (3.686(4) Å) play an important role in the 3-dimensional packing of this structure, as they connect two consecutive antiparallel chains (see Figure S1 in Supporting Information).

3.2. Enzyme Inhibition. The inhibitory activities of the compounds were evaluated against a wide panel of enzymes comprising 10 MMPs (MMP1, 2, 3, 7, 8, 9, 12, 13, 14, 16) and TACE (TNF- α converting enzyme). The results thus obtained (see Table 1) show that the inhibitory activities against these enzymes range from micromolar to low nanomolar values. The highest inhibitory activity was found for **1c** against MMP13 (IC₅₀ = 9.5 nM). Overall, this inhibitor, containing a

phenoxyphenyl-sulfonyl group, displayed the highest activities against all the tested enzymes, whereas in general, compound **1a**, containing a *p*-methoxyphenyl-sulfonyl group, demonstrated the lowest activities. Interestingly, this inhibitory profile parallels previous reports for hydroxamate-based inhibitors containing arylsulfonyl P1' groups.¹⁸

An initial attempt to rationalize these results, in terms of inhibitor–enzyme interactions, leads us to conclude that, most probably, the arylsulfonyl moiety, present in these inhibitors and in other known analogues, interacts with the cavity S1' of the enzymes in a similar manner. Compared to hydroxamic-type related inhibitors, such as compound **2** and CGS 27023A (Chart 1), the new compounds seem to be weaker MPis. While **2** displayed subnanomolar inhibitory activities against several enzymes (IC₅₀ values between 0.33–0.77 nM over MMP2, 8, 9, and 13), **1c** exhibited IC₅₀ values between 9.5–30 nM, which shows a decrease in activity from 25- to 60-fold among the tested MMPs. This fact indicates that the interactions established between this ZBG and the enzymes are weaker than those formed by the hydroxamic acid moiety.

On the other hand, although **1c** is the best inhibitor of the series, **1a** and **1b** showed more interesting selectivity profiles (see Figure S2, Supporting Information). In fact, these two compounds showed higher affinity for MMP12 over the other tested MMPs and TACE. On the other hand, **1c** showed selectivity for MMP13 over all the other MMPs, but in general with lower selectivity values than those displayed by **1a** and **1b** for MMP12.

Overall, these results suggest that the HPD moiety is an effective chelating group that may be included in the scaffold of a new class of metalloproteinase inhibitors. To selectively inhibit very similar enzymes, it is necessary to take advantage of the small differences between their protein parts. Therefore, a new approach has been hypothesized based on reducing the enormous contribution of certain binding groups, namely the ZBG, to the ligand–enzyme binding strength, at the expenses of increasing the binding interactions with other inhibitor moieties.¹³ HPD derivatives are reported to chelate metal ions with less strength than hydroxamates (with stability constants of their zinc(II) complexes ca. 1 order of magnitude lower),¹⁹ which may reveal a positive property for that strategy of increasing selectivity on metalloproteinase inhibition.

3.3. Molecular Modeling. A deep knowledge of the binding mode of these compounds within MMPs is of recognized importance for the rationalization of their activity, namely in terms of their established interactions and improving the design of new inhibitor drugs. To achieve that goal, the existence of an inhibitor–enzyme complex model may greatly ease computer-aided structure optimization by using a scaffold-constrain docking procedure, as previously reported.¹⁸ Compounds **1a–c** proved to be effective MMP inhibitors, in which the HPD moiety was expected to play the role of zinc binding group. Our research group previously conducted a complexation study of a compound

Table 1. Enzyme Inhibitory Activities (IC₅₀ Values,^a nM) of the 1-Hydroxypiperazine-2,6-dione Derivatives **1a–c and Reference Hydroxamate-Based Inhibitors**

| compd | MMP1 | MMP2 | MMP3 | MMP7 | MMP8 | MMP9 | MMP12 | MMP13 | MMP14 | MMP16 | TACE |
|------------|------|------|------|-------|------|------|-------|-------|-------|-------|-------|
| 1a | 4900 | 1200 | 3400 | 39000 | 300 | 690 | 66 | 300 | 2200 | 1100 | 33000 |
| 1b | 1300 | 240 | 3900 | nd | 67 | 660 | 19 | 52 | 3900 | 2200 | 16000 |
| 1c | 1600 | 30 | 220 | nd | 21 | 30 | 23 | 9.5 | 83 | 39 | 10000 |
| 2 | 59 | 0.50 | 6.7 | nd | 0.40 | 0.77 | nd | 0.33 | 3.9 | 1.6 | 2290 |
| CGS 27023A | 56 | 25 | 16 | 380 | 7.7 | 5.0 | nd | 5.7 | 23 | 6.8 | 160 |

^aEnzymatic data are the mean values for three independent experiments. SD are within $\pm 10\%$; nd: not determined.

containing this moiety with Zn(II), in an aqueous inorganic medium, where it showed a preference for binding to those ions via a (O,O)-bis-chelating mode.¹⁹ However, studies on the interaction of this functional group with the active site of metalloenzymes have not been reported. The most accurate way for getting information on the inhibitor–enzyme binding mode is undoubtedly via X-ray crystallographic studies of the corresponding complexes. However, in its absence, theoretical approaches have been accepted as secondary tools to produce reliable results. With this aim, we focused our attention on the binding geometry of this new ZBG (in particular, compound **1c** with MMP13) and developed a computational approach based on docking and hybrid quantum mechanical/molecular mechanical (QM/MM) calculations. Although in many cases docking calculations have been successfully applied with MMP inhibitors, the coordination of the reported ZBG with MMPs has never been predicted. Therefore, to support the reliability of the docking calculations and to have a deeper analysis of the ZBG interactions, a QM/MM approach was applied to the docking results.

The docking of compound **1c** into MMP13 was conducted to provide possible binding hypotheses of the ZBG. The ASP fitness-scoring function of GOLD software was used, as it was proven a good method for docking MMP inhibitors.¹⁸ As explained in detail in the Experimental Section, two docking runs were carried out, considering the catalytic zinc ion either with a tetrahedral or a trigonal bipyramidal coordination geometry. The two docking runs converged in a unique ligand binding mode (see Figure 2) with the ligand chelating the zinc

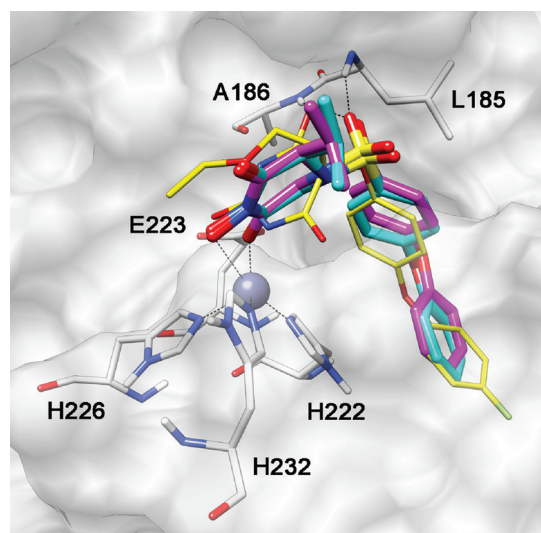


Figure 2. Superimposition of the **1c** best docking pose into MMP13, considering the catalytic zinc ion with a tetrahedral (**1c** colored light-blue) and a trigonal bipyramidal (**1c** colored magenta) coordination geometry. The crystal structures of MMP13 complexed with a pyrimidinetrione-based inhibitor (yellow, PDB entry 1YOU) is displayed as a reference structure.

ion through the 6-ketone oxygen atom and the 1-hydroxyl group of the piperazine ring, which also formed an H-bond with Glu223. The remain part of compound **1c** was placed in the binding site, similarly to many compounds containing arylsulfonyl moieties,^{20,21} with the sulfonyl O-atoms forming H-bonds with the backbone N-atoms of Leu185 and Ala186, at the entrance of the S1' cavity, while the aromatic rings were well inserted into this hydrophobic cavity.

To confirm the reliability of the docking results and to further refine the structure of the **1c**–MMP13 complex, a high-level computational modeling study was performed and is presented below.

3.4. QM/MM Dynamics Simulations. The **1c**–MMP13 complex resulting from the docking calculation was subjected to QM/MM molecular dynamics (MD) simulations. Many authors in the field of drug design have used the QM/MM approaches, with good success in finding the correct interactions in biological systems.^{22,23} In these calculations, the molecular segment with the highest interest, in terms of binding interaction, is quantum mechanically treated, while the rest of the system is treated by means of classical mechanics, thus saving considerable computational expenses. We used the QM/MM module recently implemented in AMBER10,²⁴ applying in the QM system the density functional theory-based tight-binding (DFTB) Hamiltonian model.²⁵ Because the zone of highest interest includes a metal ion (Zn), we thought this method would be the most suitable for obtaining an accurate prediction rather than a purely MM dynamics simulation. There are two ways to model the force field of this zinc ion in the MM dynamics simulations: the bonded model and the nonbonded model. In the bonded model, the commonly used bonded terms describe the coordinates between zinc and ligand/MMP, including bond stretching. In the nonbonded approach, van der Waals and nonbonded electrostatic terms are used to model the zinc–ligand/MMP interactions. The bonded model is quite efficient but requires the parametrization of the interactions between the zinc ion and the ligand/MMP.²⁶ On the other hand, the nonbonded method is highly sensitive to the choice of the electrostatic model and can suffer from an inability to retain a low coordination number. Furthermore, with the AMBER force field, the nonbonded approach generally fails to give the correct coordination number, even when the long-range electrostatic interactions are correctly accounted for using an infinite cutoff.^{27,28}

For these reasons, we preferred to adopt a hybrid QM/MM approach that would be able to avoid the problems correlated with the MM dynamic simulations. As already mentioned, the QM/MM module was recently reported and, up to now, has never been used to analyze inhibitor–MMP complexes. Therefore, prior to evaluating our **1c**–MMP13 binding hypothesis, we tested the reliability of the method by launching QM/MM simulations on two MMP13 crystal structures, one containing a hydroxamate inhibitor (4-[4-(4-chloro-phenoxy)-benzenesulfonylmethyl]-tetrahydropyran-4-carboxylic acid hydroxyamide, PDB entry 830C²⁹) and another containing a barbiturate (5-(2-ethoxyethyl)-5-[4-(4-fluorophenoxy)phenoxy]pyrimidine-2,4,6(1H,3H,5H)-trione, PDB entry 1YOU³⁰). These were chosen based on the similarity between our ZBG and both hydroxamate and barbiturate groups. Each structure, in an explicit solvent environment, was subjected to two minimization and three MD steps, the last one consisting of 4 ns of QM/MM MD simulation (see the Experimental Section for details).

As shown in Figure 3, both complexes seemed to be stable during the simulations. By analyzing the root-mean-square deviation (rmsd) of all the heavy atoms from the X-ray structures, we observed an initial increase due to the equilibration of the system, followed, after 500 ps, by a stabilization of the rmsd value around 1.1 Å. Regarding the geometry of the ligand, we analyzed the rmsd of the position of the ligands with respect to the X-ray structures during the simulation. Figure 3 shows that both ligands demonstrated rmsd values between 0.3 and 0.7 Å.

From the X-ray structures of the complexes, we observed that the two ligands formed four H-bonds with MMP13. As shown

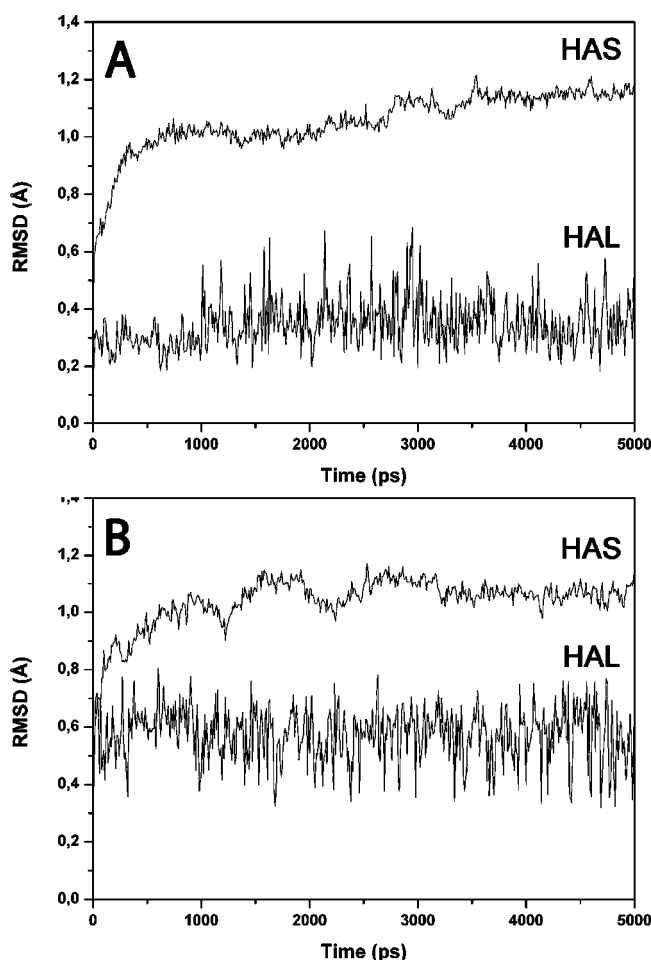
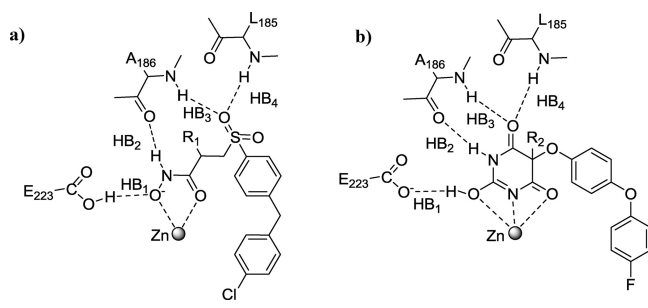


Figure 3. Analysis of the QM/MM simulations for the hydroxamic (A) and barbiturate-based compounds (B) complexed with MMP13. The plots show the rmsd during the simulations of the heavy atoms of the whole system (upper curve, HAS) and of the heavy atoms of the ligands (downer curves, HAL) from the starting model structures.

in Table 2, both compounds interacted with Leu185, Ala186, and Glu223, and these interactions were maintained during the

Table 2. H-Bond Analysis during the 5 ns MD Simulation for the Hydroxamate (a) and Barbiturate (b) Based Ligands



| H-bond | distance (Å) | % occupied | H-bond | distance (Å) | % occupied |
|--------|--------------|------------|--------|--------------|------------|
| HB1 | 2.7 | 99.6 | HB1 | 2.6 | 87.4 |
| HB2 | 3.0 | 68.4 | HB2 | 2.8 | 100.0 |
| HB3 | 3.3 | 43.0 | HB3 | 3.2 | 71.3 |
| HB4 | 3.0 | 93.8 | HB4 | 2.9 | 92.9 |

MD simulation. Finally, the complexes obtained by minimizing the average structure of the last 4 ns of MD (corresponding to

the QM/MM MD), showed that all four H-bonds were present and the ligand geometries were quite similar to the X-ray starting structures (see Figure S3 in the Supporting Information).

Once we tested and validated the QM/MM simulation approach for modeling ligands–MMP complexes, we subjected the 1c–MMP13 complex obtained from the docking studies to the same protocol used above. Figure 4 shows that the 1c-complex

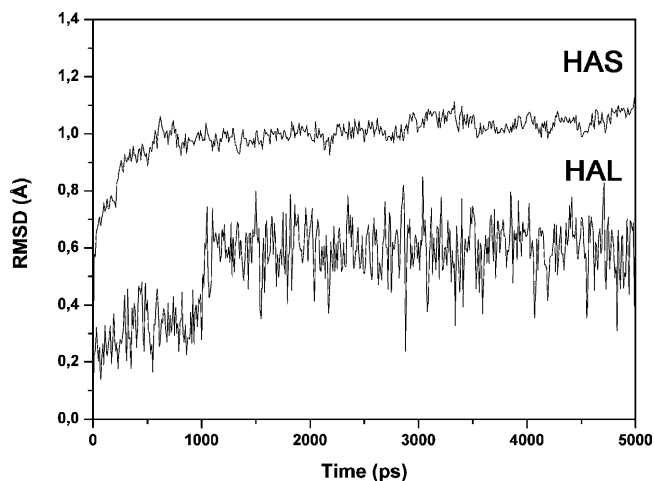


Figure 4. Analysis of the QM/MM simulations for the 1c–MMP13 complex. The plot shows the rmsd during the simulations of the heavy atoms of the whole system (upper curve, HAS) and of the heavy atoms of 1c (downward curves, HAL) from the starting model structures.

seemed to be stable during the simulations. The rmsd of the heavy atoms from the X-ray structures was very similar to those reported for the hydroxamate and barbiturate derivatives. The rmsd presented a small initial increase, but after 500 ps, remained between 0.9 and 1.1 Å for the three systems. Concerning the geometry of the ligand, after an initial increase, it showed a rmsd value between 0.4 and 0.7 Å in the last 4 ns.

Figure 5 shows the minimized average structure of the last 4 ns of the MD simulation of the 1c–MMP13 complex. The zinc

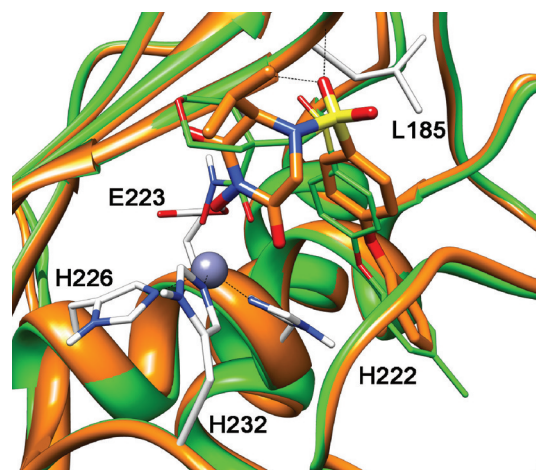


Figure 5. Minimized average structures resulting from the MD simulation of the 1c–MMP13 complex (orange) superimposed with the crystal structures of MMP13 complexed with a hydroxamate inhibitor (green, PDB entry 830C).

ion displayed a trigonal bipyramidal geometry, chelated by the ligand through the 6-ketone O-atom and the 1-hydroxyl group

of the piperazine ring, which also formed an H-bond with the carboxylate of Glu223. With regards to the sulfonyl O-atom, it formed H-bonds with the backbone N-atoms of Leu185 and Ala186 at the entrance of the S1' cavity, while the aromatic rings were inserted into this hydrophobic cavity. As shown in Table S1 in the Supporting Information, the H-bond analysis of the simulation confirmed the interactions described above, as the three H-bonds were maintained during the MD trajectory.

The comparison between the docking and the QM/MM results for the **1c**–MMP13 complex highlighted the existence of considerable differences on the ZBG disposition. As shown in Figure S4A in the Supporting Information, the HPD resulting from the QM/MM calculations was rotated about 90° with respect to the ZBG docking disposition. A further analysis of the GOLD docking poses for **1c** revealed that, considering a trigonal bipyramidal coordination geometry for the zinc, the pose ranked as tenth showed a disposition very similar to the QM/MM results (see Supporting Information Figure S4B). These data support the hypothesis that GOLD is able to find the correct binding disposition of the HPD moiety but is unable to rank it as the preferred disposition and is therefore in agreement with the use of QM/MM calculations for refining the starting docking results.

The final average structure of the **1c**–MMP13 complex, arising from the hybrid QM/MM MD simulation, gave extra evidence of the potential of the HPD moiety as an effective ZBG to be used in the inhibition of MMPs and other metalloproteinases. Beyond the modification of the 4-arylsulfonyl substituent that is known to modulate activity against the different MMP subtypes,^{31,32} a structure optimization can still be performed through substitution at the 3- and 5-positions of the HPD ring. As shown in Figure S5A in the Supporting Information, the superimposition of the **1c**–MMP13 complex with the crystal structure of MMP13 complexed with a potent pyrimidinetrione-based inhibitor highlights the fact that the 3-position of HPD corresponds to the C-5 position of the pyrimidinetrione ring. Previous studies on the C-5 substitution of the pyrimidinetrione-based inhibitor showed that this portion of the ligands interacts with the solvent-exposed S1 region of the MMPs, which is useful for modulating their activity.^{30,33} Furthermore, an opportune substitution at the 3-position of HPD could also mimic the 5-position of hydantoin-based MMP inhibitors (see Figure S5B in the Supporting Information), which can bear large substituents that are able to drastically change the MMP inhibition activity.^{34,35} Finally, the superimposition between the **1c**–MMP13 complex and MMP3 complexed with a potent heterocycle-based inhibitor (see Figure S5C in the Supporting Information), highlights the fact that the 5-position of HPD could be profitably used to explore the S2' region, which is considered a useful feature for modulating the activity and selectivity of MPis.³⁶

3.5. QM Optimization. To confirm the results obtained by the docking-QM/MM approach, QM optimization of the interaction between the ZBG and MMP13 was carried out. The catalytic zinc binding region was retrieved from the minimized average structure of the last 4 ns of **1c**–MMP13 MD simulation and submitted to purely quantum mechanics optimization, using Gaussian software, with the B3LYP chemical model and the LANL2DZ and the 6-31++G(d,p) basis set. Simplifications on the binding site were made, and only the main atoms around the ZBG were included, while the phenoxyphenyl group of **1c** was reduced to a simpler methoxyphenyl (see Experimental Section). The QM

optimizations converged into solutions similar to the structure obtained from the QM/MM calculation. In Figure 6, the final

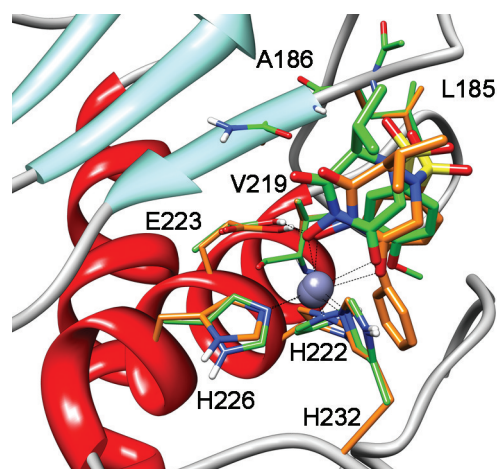


Figure 6. Superimposition of the minimized average structures resulting from the **1c**–MMP13 simulation (orange) and the simplified model optimized with the QM method (green).

structures of the QM optimization (6-31++G(d,p) basis set) and the average of the QM/MM MD simulation of **1c**–MMP13 are superimposed. These two structures are very close to each other, also when considering the ZBG, with a rmsd of 0.8 Å for the heavy atoms of the HPD ring. Such facts emphasize the accuracy of our computational method when investigating the binding mode of the new ZBG type.

4. CONCLUSIONS

A new set of compounds containing a novel zinc-binding moiety was identified and proved to be effective MMP inhibitors, with the highest inhibition observed for compound **1c** toward MMP13 (IC₅₀ value of 9.5 nM). The 1-hydroxypiperazine-2,6-dione (HPD) moiety presented itself as a valid and promising ZBG to be used in a new class of metalloproteinase inhibitors. A theoretical approach was employed to analyze the binding mode of new types of inhibitors with metalloproteins and, in particular, to disclose the binding geometry of compound **1c** with MMP13. The resulting structure was suitable for fast docking calculations using scaffold constraints, which can be applied to the design optimization of new derivatives with improved inhibitory profiles toward the target enzymes. The general structure of the new inhibitors (Chart 1) has three main feature points available for optimization: the aromatic group “Ar”, interacting within the hydrophobic pocket S1', the substituent group at 3-position of the HPD ring interacting with the S1 region, and the substituent group at 5-position of the ZBG ring pointing toward the S2' region.

5. EXPERIMENTAL SECTION

5.1. Synthesis of the Compounds. *General Methods and Materials.* Analytical grade reagents were purchased from Sigma-Aldrich, Fluka and Acros and were used as supplied. Solvents were dried according to standard methods.³⁷ The chemical reactions were monitored by TLC using alumina plates coated with silica gel 60 F₂₅₄ (Merck). The purity of the compounds was determined by HPLC, and it was found to be higher than 95% for all target compounds (see Supporting Information for details). The melting points were measured with a Leica Galen III hot stage apparatus and are uncorrected. The ¹H NMR spectra were recorded on a Bruker

AVANCE III 300 MHz spectrometer, and the ^{13}C NMR spectra were measured on a Bruker AVANCE III 400 MHz spectrometer, all at room temperature. Chemical shifts (δ) are reported in ppm from the standard internal reference tetramethylsilane (TMS) for the organic solvents, sodium 3-(trimethylsilyl)-[2,2,3,3- d_4]-propionate (DSS) for D_2O solutions, or the solvent peak for the ^{13}C NMR. The following abbreviations are used: s = singlet, d = doublet, t = triplet, m = multiplet. For the NMR-monitored stability studies, solutions of **1a** (ca. 15 mM) were prepared in D_2O , and the pD (pD = $-\log [D^+]$) was adjusted by addition of DCl and KOD solutions in D_2O . The mass spectra (FAB) were performed in a VG TRIO-2000 GC/MS instrument. The elemental analyses were performed for the target compounds (**1a–c**) on a Fisons EA1108 CHN/F/O instrument and were within the limit of $\pm 0.4\%$.

Preparation of Compounds 3a–3c. (*R*)-1-(Benzyloxy)-3-isopropyl-4-(4-methoxyphenylsulfonyl)piperazine-2,6-dione (**3a**). To a solution of (*R*)-2-(*N*-(1-(benzyloxyamino)-3-methyl-1-oxobutan-2-yl)-4-methoxyphenylsulfonamido)-acetic acid (**2a**), obtained as previously reported¹⁸ (0.200 g, 0.44 mmol), in dry THF (30 mL) at 0 °C was added ethylchloroformate (ECF, 0.050 mL, 0.53 mmol) and dry *N*-methylmorpholine (NMM, 0.058 mL, 0.53 mmol); the mixture was stirred for 1 h, and then it was evaporated. The residue was taken into 1:1 ethyl ether/ethyl acetate (40 mL), and this solution was washed with 0.1 M HCl (2 \times 40 mL), 5% NaOH (2 \times 40 mL), and water (40 mL). After drying the organic phase over anhydrous Na_2SO_4 , solvent evaporation under vacuum afforded the pure product as a white solid (0.112 g, 59% yield); mp 75–76 °C. ^1H NMR (CDCl_3), δ : 7.74 (d, J = 8.7 Hz, 2H, ArH), 7.35 (s, 5H, PhH), 7.00 (d, J = 8.4 Hz, 2H, ArH), 4.73 (d, J = 19.8 Hz, 1H, NCH_2CON), 4.39 (d, J = 9.0 Hz, 1H, CH_2Ph), 4.32 (d, J = 9.0 Hz, 1H, CH_2Ph), 4.22 (d, J = 10.2 Hz, 1H, $\text{NCH}(\text{iPr})\text{CON}$), 4.05 (d, J = 19.5 Hz, 1H, NCH_2CON), 3.77 (s, 3H, OCH_3), 1.99–1.90 (m, 1H, $\text{CH}(\text{CH}_3)_2$), 1.10 (d, J = 6.3 Hz, 3H, CHCH_3), 1.03 (d, J = 6.9 Hz, 3H, CHCH_3); m/z (FAB): 433 ($\text{M} + \text{H}$)⁺, 455 ($\text{M} + \text{Na}$)⁺.

(*R*)-1-(Benzyloxy)-4-(biphenyl-4-ylsulfonyl)-3-isopropylpiperazine-2,6-dione (**3b**). White solid (40% yield); mp 130–133 °C. ^1H NMR (CDCl_3), δ : 7.88 (d, J = 8.1 Hz, 2H, ArH), 7.74 (d, J = 8.4 Hz, 2H, ArH), 7.46–7.38 (m, 5H, ArH), 7.25 (s, 5H, ArH), 4.79 (d, J = 19.8 Hz, 1H, NCH_2CON), 4.32–4.22 (m, 3H, CH_2Ph , $\text{NCH}(\text{iPr})\text{CON}$), 4.10 (d, J = 19.5 Hz, 1H, NCH_2CON), 2.6–1.05 (m, 1H, $\text{CH}(\text{CH}_3)_2$), 1.14 (d, J = 6.6 Hz, 3H, CHCH_3), 1.07 (d, J = 6.3 Hz, 3H, CHCH_3); m/z (FAB): 479 ($\text{M} + \text{H}$)⁺, 501 ($\text{M} + \text{Na}$)⁺.

(*R*)-1-(Benzyloxy)-3-isopropyl-4-(4-phenoxyphenylsulfonyl)piperazine-2,6-dione (**3c**). White hygroscopic solid (44% yield). ^1H NMR (CDCl_3), δ : 7.73 (d, J = 9.0 Hz, 2H, ArH), 7.43–7.38 (m, 4H, ArH), 7.25–7.15 (m, 4H, ArH), 7.03 (d, J = 9.0 Hz, 2H, ArH), 6.83 (d, J = 7.8 Hz, 2H, ArH), 4.73 (d, J = 18.0 Hz, 1H, NCH_2CON), 4.44 (d, J = 8.7 Hz, 1H, CH_2Ph), 4.39 (d, J = 8.4 Hz, 1H, CH_2Ph), 4.23 (d, J = 10.2 Hz, 1H, $\text{NCH}(\text{iPr})\text{CON}$), 4.07 (d, J = 19.5 Hz, 1H, NCH_2CON), 2.01–1.92 (m, 1H, $\text{CH}(\text{CH}_3)_2$), 1.12 (d, J = 6.3 Hz, 3H, CHCH_3), 1.05 (d, J = 6.6 Hz, 3H, CHCH_3); m/z (FAB): 495 ($\text{M} + \text{H}$)⁺, 517 ($\text{M} + \text{Na}$)⁺.

Preparation of Compounds 1a–1c. (*R*)-1-Hydroxy-3-isopropyl-4-(4-methoxyphenylsulfonyl)piperazine-2,6-dione (**1a**). The general method for benzyl deprotection by catalytic hydrogenolysis was followed: to a solution of **3a** (0.100 g, 0.23 mmol) in methanol (10 mL), 10% Pd/C (0.025 g) was added and the suspension was stirred for 3 h under H_2 (1.5 bar). After filtration and solvent removal, final recrystallization from ethyl ether/petroleum ether afforded the pure product as a white hygroscopic solid (0.076 g, 96% yield). ^1H NMR (CDCl_3), δ : 7.68 (d, J = 8.7 Hz, 2H, ArH), 6.98 (d, J = 8.7 Hz, 2H, ArH), 4.75 (d, J = 19.5 Hz, 1H, NCH_2CON), 4.27 (d, J = 9.9 Hz, 1H, $\text{NCH}(\text{iPr})\text{CON}$), 4.11 (d, J = 19.5 Hz, 1H, NCH_2CON), 3.86 (s, 3H, OCH_3), 2.13–2.02 (m, 1H, $\text{CH}(\text{CH}_3)_2$), 1.15–1.10 (m, 6H, $\text{CH}(\text{CH}_3)_2$). ^{13}C NMR (CDCl_3), δ : 164.5, 164.1 (2 peaks, C=O), 162.5, 128.4, (2 peaks, *para*- and *ipso*-Ar-C), 129.3, 115.2 (2 peaks, *ortho*- and *meta*-Ar-C), 64.0 ($\text{CCH}(\text{CH}_3)_2$), 55.9 (OCH_3), 45.5 (NCH_2CO), 29.4 ($\text{CH}(\text{CH}_3)_2$), 20.1, 19.2 (2 peaks, $\text{CH}(\text{CH}_3)_2$); m/z (FAB): 343 ($\text{M} + \text{H}$)⁺, 365 ($\text{M} + \text{Na}$)⁺.

(*R*)-4-(Biphenyl-4-ylsulfonyl)-1-hydroxy-3-isopropylpiperazine-2,6-dione (**1b**). White solid (86% yield); mp 164–165 °C. ^1H NMR (CDCl_3), δ : 7.81 (d, J = 8.4 Hz, 2H, ArH), 7.74 (d, J = 9.0 Hz, 2H, ArH), 7.59 (d, J = 6.6 Hz, 2H, ArH), 7.51–7.43 (m, 3H, ArH), 4.80 (d, J = 19.5 Hz, 1H, NCH_2CON), 4.34 (d, J = 9.6, 1H, $\text{NCH}(\text{iPr})\text{CON}$), 4.15 (d, J = 19.5 Hz, 1H, NCH_2CON), 2.17–2.03 (m, 1H, $\text{CH}(\text{CH}_3)_2$), 1.18–1.12 (m, 6H, $\text{CH}(\text{CH}_3)_2$). ^{13}C NMR (CDCl_3), δ : 164.3, 161.6 (2 peaks, C=O), 147.2, 138.8, 135.5, 129.0, (4 peaks, *para*- and *ipso*-Ar-C), 129.3, 128.6, 127.55, 127.52 (4 peaks, *ortho*- and *meta*-Ar-C), 64.0 ($\text{CCH}(\text{CH}_3)_2$), 45.6 (NCH_2CO), 29.5 ($\text{CH}(\text{CH}_3)_2$), 20.2, 19.2 (2 peaks, $\text{H}(\text{CH}_3)_2$); m/z (FAB): 389 ($\text{M} + \text{H}$)⁺, 411 ($\text{M} + \text{Na}$)⁺.

(*R*)-1-Hydroxy-3-isopropyl-4-(4-phenoxyphenylsulfonyl)piperazine-2,6-dione (**1c**). White hygroscopic solid (96% yield). ^1H NMR (CDCl_3), δ : 7.68 (d, J = 9.0 Hz, 2H, ArH), 7.40 (t, 2H, ArH), 7.42 (t, J = 7.8 Hz, 1H, ArH), 7.06–7.03 (m, 4H, ArH), 4.75 (d, J = 19.8 Hz, 1H, NCH_2CON), 4.28 (d, J = 9.6 Hz, 1H, $\text{NCH}(\text{iPr})\text{CON}$), 4.12 (d, J = 19.2 Hz, 1H, NCH_2CON), 2.14–2.03 (m, 1H, $\text{CH}(\text{CH}_3)_2$), 1.16–1.11 (m, 6H, $\text{CH}(\text{CH}_3)_2$). ^{13}C NMR (CDCl_3), δ : 164.5, 162.7 (2 peaks, C=O), 162.1, 154.7, 130.0, 125.2, (4 peaks, *para*- and *ipso*-Ar-C), 130.2, 129.2, 120.3, 118.3 (4 peaks, *ortho*- and *meta*-Ar-C), 63.9 ($\text{CCH}(\text{CH}_3)_2$), 45.4 (NCH_2CO), 29.2 ($\text{CH}(\text{CH}_3)_2$), 20.0, 19.0 (2 peaks, $\text{CH}(\text{CH}_3)_2$); m/z (FAB): 427 ($\text{M} + \text{Na}$)⁺, 405 ($\text{M} + \text{H}$)⁺.

5.2. X-ray Diffraction. The crystallographic data are displayed in Table 3. Colorless crystals of compound **1b** were obtained from slow

Table 3. Crystallographic Data for Compound 1b

| | 1b |
|--|--|
| chemical formula | $\text{C}_{19}\text{H}_{20}\text{N}_2\text{O}_5\text{S}$ |
| M_r | 388.43 |
| temperature/K | 150(2) |
| wavelength/Å | 0.71069 |
| morphology, color | plate, colorless |
| crystal size/mm | 0.20 \times 0.12 \times 0.04 |
| crystal system | monoclinic |
| space group | $P2_1$ |
| $a/\text{Å}$ | 7.1064(5) |
| $b/\text{Å}$ | 7.8402(6) |
| $c/\text{Å}$ | 16.3344(12) |
| β/deg | 94.589(4) |
| $V/\text{Å}^3$ | 907.16(12) |
| Z | 2 |
| calcd density/ $\text{mg}\cdot\text{m}^{-3}$ | 1.422 |
| absorption coefficient/ mm^{-1} | 0.213 |
| θ min/deg | 1.25 |
| θ max/deg | 27.94 |
| reflins collected/unique | 10231/4294 |
| R_{int} | 0.0506 |
| GoF | 0.988 |
| threshold expression | $I > 2\sigma(I)$ |
| R_1 (obsd) | 0.0487 |
| wR_2 (all) | 0.0967 |

evaporation of a dichloromethane solution of the compound. The single crystals were mounted on a cryoloop using Fomblin as protective oil. Single-crystal X-ray diffraction data was collected at 150 K on a Bruker AXS-KAPPA APEX II diffractometer with graphite-monochromated radiation (Mo $K\alpha$, λ = 0.71069 Å). X-ray data collection was monitored by SMART program (Bruker, 2003). All the data were corrected for Lorentzian, polarization, and absorption effects using SAINT³⁸ program. SIR97³⁹ was used for structure solution, and SHELXL-97⁴⁰ was used for full matrix least-squares refinement on F2. All non-hydrogen atoms were refined anisotropically. All H atoms were added in calculated positions and refined riding on their resident

atoms. ORTEP 3.2⁴¹ was used for molecular representations, and MERCURY 2.3⁴² was used for packing diagrams.

5.3. Enzyme Inhibition.⁴³ Recombinant human progelatinase A (pro-MMP2) and B (pro-MMP9), pro-MMP8, MMP16, and MMP14 catalytic domains were a kind gift of Prof. Gillian Murphy (Department of Oncology, University of Cambridge, UK). Pro-MMP1, pro-MMP3, pro-MMP7, pro-MMP13, and TACE (ADAM-17) were purchased from Calbiochem. Pro-MMP12 was purchased by R&D Systems.

Proenzymes were activated immediately prior to use with *p*-aminophenylmercuric acetate (APMA, 2 mM for 1 h at 37 °C for MMP2 and MMP8, 1 mM for 1 h at 37 °C for MMP9 and MMP13, 2 mM for 2 h at 37 °C for MMP1, 3.3 mM for 2 h at 37 °C for MMP7). Pro-MMP3 was activated with trypsin, 5 µg/mL for 30 min at 37 °C, followed by soybean trypsin inhibitor (SBTI, 62 µg/mL). Pro-MMP12 was autoactivated by incubating in the fluorimetric assay buffer (FAB: Tris 50 mM, pH = 7.5, NaCl 150 mM, CaCl₂ 10 mM, Brij 35 0.05%, and DMSO 1%) for 30 h at 37 °C.

For the assay measurements, the inhibitor stock solutions (DMSO, 10 mM) were diluted at seven different concentrations for each MMP in FAB. The activated enzyme (final concentration 0.5 nM for MMP2, 1.3 nM for MMP9, 1.5 nM for MMP8, 0.3 nM for MMP13, 5 nM for MMP3, 1.3 nM for MMP7, 1.0 nM for MMP14 cd, 15 nM for MMP16 cd, 2.0 nM for MMP1, 1.0 nM for MMP12, and 7.5 nM for TACE) and inhibitor solutions were incubated in the assay buffer for 4 h at 25 °C. After the addition of 200 µM solution of the fluorogenic substrate Mca-Arg-Pro-Lys-Pro-Val-Glu-Nva-Trp-Arg-Lys(Dnp)-NH₂ (Sigma) for MMP3 and Mca-Lys-Pro-Leu-Gly-Leu-Dap(Dnp)-Ala-Arg-NH₂ (Bachem) for all the other enzymes in DMSO (final concentration 2 µM), the hydrolysis was monitored every 15 s for 20 min, recording the increase in fluorescence ($\lambda_{\text{ex}} = 325$ nm, $\lambda_{\text{em}} = 395$ nm) using a Molecular Devices SpectraMax Gemini XS plate reader. The assays were performed in a total volume of 200 µL per well in 96-well microtiter plates (Corning, black, NBS). Control wells lack inhibitor. The MMP inhibition activity was expressed in relative fluorescent units (RFU). Percent of inhibition was calculated from control reactions without the inhibitor. IC₅₀ was determined using the formula: $V_i/V_0 = 1/(1 + [I]/IC_{50})$, where V_i is the initial velocity of substrate cleavage in the presence of the inhibitor at concentration [I] and V_0 is the initial velocity in the absence of the inhibitor. Results were analyzed using SoftMax Pro software⁴⁴ and GraFit software.⁴⁵

5.4. Docking of Compound 1c. The ligand structure was built using Maestro 9.0⁴⁶ and it was minimized with Macromodel 9.7.⁴⁷ The conjugated gradient method was applied, until a convergence value of 0.05 kJ/Å·mol was reached, using the MMFFs force field and a water environment model (generalized-Born/surface-area model), with a distance-dependent dielectric constant of 1.0. The minimized ligand was then subjected to a conformational search of 100 steps, using an algorithm based on the Monte Carlo method, with the same force field and parameters used in the minimization. The structure of the MMP13 was extracted from the RCSB Protein Data Bank⁴⁸ (PDB code 830C²⁹). Hydrogen atoms were added by means of Maestro, and the region of interest used by the docking program GOLD version 4.0⁴⁹ was defined in order to contain the residues within 15 Å from the original position of the ligand in the X-ray structure. In the docking calculations, the catalytic zinc ion was set to have either a tetrahedral or a trigonal bipyramidal coordination geometry. The “allow early termination” option was deactivated. The clusterization was set for an rmsd limit of 0.75 Å between the different docking solutions. The remaining GOLD default parameters were used, and the ligand was submitted to 100 genetic algorithm runs by applying the ASP fitness scoring function. The clustered structures obtained from the two docking runs were then compared.

5.5. QM/MM Simulations. All simulations were performed using AMBER 10.²⁴ Molecular dynamics (MD) simulations were carried out using the parm03 force field at 300 K. Two MMP13 structures complexed with inhibitors (a hydroxamate, PDB entry 830C;²⁹ a barbiturate, PDB entry 1YOU³⁰) were taken from the RCSB Protein Data Bank.⁴⁸ The complexes were placed in a rectangular parallelepiped water box, an explicit solvent model for water, TIP3P, was used, and the complex was solvated with a 10 Å water cap. Sodium

ions were added as counterions to neutralize the system. Prior to the MD, two minimization steps were carried out. In the first stage, the protein was fixed using a harmonic force constant of 500 kcal/mol·Å² and only the positions of the water molecules were minimized. In the second stage, the entire system was minimized by applying a harmonic force constraint of 15 kcal/mol·Å² on the α -carbons, the two zinc ions, and the corresponding coordinating atoms (from the protein and the ligand). The first minimization consisted of 5000 steps with a combined algorithm, namely the sequential use of Steepest Descent (SD) and Conjugate Gradient (CG) methods, for the first 1000 and the last 4000 steps, respectively, while the second one consisted of 9000 steps with 1000 SD and 8000 CG steps.

Particle mesh Ewald⁵⁰ (PME) electrostatics and periodic boundary conditions were used in the simulation. The MD trajectory was conducted using the minimized structure as the starting conformation. The time step of the simulations was 2.0 fs with a cutoff of 10 Å for the nonbonded interaction, and SHAKE was employed to keep rigid all bonds involving hydrogen atoms. Constant volume was carried out for 200 ps, during which the temperature was raised from 0 to 300 K (using the Langevin dynamics method). Next, under constant-pressure, an 800 ps MD simulation was carried out at 300 K. During these two MD steps, the same constraints were applied as described for the second minimization step. General Amber force field (GAFF) parameters were assigned to the ligands, while partial charges were calculated using the AM1-BCC method as implemented in the Antechamber suite of AMBER 10. A 4 ns MD simulation was then performed using the hybrid quantum mechanical/molecular mechanical (QM/MM) method of AMBER 10. The quantum mechanics (QM) region was described by the DFTB theory²⁵ and contained the catalytic zinc ion, the imidazole rings of the three His residues surrounding it, the Glu223 carboxylic group, and the ZBG (hydroxamic acid and barbiturate moiety). Aside from those atoms within the QM region, the same constraints of the previous MD were applied. In the molecular mechanics (MM) region, the parameters were the same as in the previous MD, but in the QM region, the PME algorithm was deactivated; and this region's charge was defined as 1. This MD simulation protocol was also applied to the MMP13–compound 1c complex that resulted from the docking study.

5.6. QM Optimization. Geometry optimization was performed by means of quantum mechanical calculations derived from the Gaussian 03W software.⁵¹ The minimized average structure of the last 4 ns of the MD simulation of the MMP13–compound 1c complex was used as the starting structure. Only the most important residues of the binding site region were taken into account, i.e. the catalytic zinc ion, the imidazole rings of the three His residues surrounding it, the Glu223 carboxylic group, Leu185, Ala186, Val219, and the ligand 1c, with its portion 4-phenoxyphenylsulfonfyl substituted by a smaller 4-methoxyphenylsulfonfyl. The QM calculation was carried out using the B3LYP chemical model and two different basis sets (i.e., the LANL2DZ and the 6-31++G(d,p) basis set). A direct self-consistent field (SCF) method with a SCF convergence criterion of 10⁻⁵ was used. The backbone atoms of the residues were kept fixed.

■ ASSOCIATED CONTENT

📄 Supporting Information

Extra data on the crystallographic structure, enzyme inhibition, QM/MM dynamic structure, and compounds characterization. This material is available free of charge via the Internet at <http://pubs.acs.org>.

■ AUTHOR INFORMATION

Corresponding Authors

*For M.A.S.: phone, 00351-218419273; fax, 00351-218464455; e-mail, masantos@ist.utl.pt. For T.T.: phone, 0039-0502219595; fax, 0039-0502219605; e-mail, tuccinardi@farm.unipi.it.

ACKNOWLEDGMENTS

We acknowledge the Portuguese Fundação para a Ciência e Tecnologia (FCT) for financial support, with the postdoc grant SFRH/BPD/29874/2006 (S.M.M.) and the Ph.D. grant SFRH/BD/40474/2007 (V.A.). We also thank the Portuguese NMR Network (IST-UTL Center) for providing access to the NMR facility. The mass spectra were obtained at the IST Node, which is part of the National Mass Spectrometry Network (RNEM) created by the FCT. We are also thankful to Prof. Teresa Duarte for the helpful discussions on the X-ray analysis. Molecular graphics images were produced using the UCSF Chimera package from the Resource for Biocomputing, Visualization, and Informatics at the University of California, San Francisco (supported by NIH grant P41 RR01081).

ABBREVIATIONS USED

HPD, 1-hydroxypiperazine-2,6-dione; MMP, matrix metalloproteinase; QM, quantum mechanics; MM, molecular mechanics; ZBG, zinc-binding group; MPI, MMP inhibitor; ECF, ethylchloroformate; TBTU, *O*-(benzotriazol-1-yl)-*N,N,N',N'*-tetramethyluronium tetrafluoroborate; MD, molecular dynamics; DFTB, density functional theory-based-tight-binding; rmsd, root-mean-square deviation

REFERENCES

- (1) Whittaker, M.; Floyd, C. D.; Brown, P.; Gearing, A. J. Design and therapeutic application of matrix metalloproteinase inhibitors. *Chem. Rev.* **1999**, *99*, 2735–2776.
- (2) Egeblad, M.; Werb, Z. New functions for the matrix metalloproteinases in cancer progression. *Nature Rev. Cancer* **2002**, *2*, 161–174.
- (3) Dormán, G.; Cseh, S.; Hajdú, I.; Barna, L.; Kónya, D.; Kupai, K.; Kovács, L.; Ferdinandy, P. Matrix metalloproteinase inhibitors: a critical appraisal of design principles and proposed therapeutic utility. *Drugs* **2010**, *70*, 949–964.
- (4) Rao, B. G. Recent developments in the design of specific matrix metalloproteinase inhibitors aided by structural and computational studies. *Curr. Pharm. Des.* **2005**, *11*, 295–322.
- (5) Coussens, L. M.; Fingleton, B.; Matrisian, L. M. Matrix metalloproteinase inhibitors and cancer: trials and tribulations. *Science* **2002**, *295* (5564), 2387–2392.
- (6) Overall, C. M.; Kleifeld, O. Tumour microenvironment—opinion: validating matrix metalloproteinases as drug targets and anti-targets for cancer therapy. *Nature Rev. Cancer* **2006**, *6*, 227–239.
- (7) Pirard, B. Insight into the structural determinants for selective inhibition of matrix metalloproteinases. *Drug. Discovery Today* **2007**, *12*, 640–646.
- (8) Flipo, M.; Charton, J.; Hocine, A.; Dassonneville, S.; Deprez, B.; Deprez-Poulain, R. Hydroxamates: relationships between structure and plasma stability. *J. Med. Chem.* **2009**, *52*, 6790–6802.
- (9) Puerta, D. T.; Lewis, J. A.; Cohen, S. M. New beginnings for matrix metalloproteinase inhibitors: identification of high-affinity zinc-binding groups. *J. Am. Chem. Soc.* **2004**, *126*, 8388–8389.
- (10) MacPherson, L. J.; Bayburt, E. K.; Capparelli, M. P.; Carroll, B. J.; Goldstein, R.; Justice, M. R.; Zhu, L.; Hu, S.; Melton, R. A.; Fryer, L.; Goldberg, R. L.; Doughty, J. R.; Spirito, S.; Blancuzzi, V.; Wilson, D.; O'Byrne, E. M.; Ganu, V.; Parker, D. T. Discovery of CGS 27023A, a non-peptidic, potent, and orally active stromelysin inhibitor that blocks cartilage degradation in rabbits. *J. Med. Chem.* **1997**, *40*, 2525–2532.
- (11) Morrison, C. J.; Butler, G. S.; Rodriguez, D.; Overall, C. M. Matrix metalloproteinase proteomics: substrates, targets, and therapy. *Curr. Opin. Cell Biol.* **2009**, *21*, 645–653.
- (12) Strongin, A. Y. Proteolytic and non-proteolytic roles of membrane type-1 matrix metalloproteinase in malignancy. *Biochim. Biophys. Acta* **2010**, *1803*, 133–141.
- (13) Overall, C. M.; Kleifeld, O. Towards third generation matrix metalloproteinase inhibitors for cancer therapy. *Br. J. Cancer* **2006**, *94*, 941–946.
- (14) Saghatelian, A.; Jessani, N.; Joseph, A.; Humphrey, M.; Cravatt, B. F. Activity-based probes for the proteomic profiling of metalloproteases. *Proc. Natl. Acad. Sci. U.S.A.* **2004**, *101*, 10000–10005.
- (15) Puerta, D. T.; Griffin, M. O.; Lewis, J. A.; Romero-Perez, D.; Garcia, R.; Villarreal, F. J.; Cohen, S. M. Heterocyclic zinc-binding groups for use in next-generation matrix metalloproteinase inhibitors: potency, toxicity, and reactivity. *J. Biol. Inorg. Chem.* **2006**, *11*, 131–138.
- (16) Ledour, G.; Moroy, G.; Rouffet, M.; Bourguet, E.; Guillaume, D.; Decarme, M.; Elmourabit, H.; Auge, F.; Alix, A. J.; Laronze, J. Y.; Bellon, G.; Hornebeck, W.; Sapi, J. Introduction of the 4-(4-bromophenyl)benzenesulfonyl group to hydrazide analogs of Ilomastat leads to potent gelatinase B (MMP-9) inhibitors with improved selectivity. *Bioorg. Med. Chem.* **2008**, *16*, 8745–8759.
- (17) Li, D. L.; Zheng, Q. C.; Fang, X. X.; Ji, H. T.; Yang, J. G.; Zhang, H. X. Theoretical study on potency and selectivity of novel non-peptide inhibitors of matrix metalloproteinases MMP-1 and MMP-3. *Polymer* **2008**, *49*, 3346–3351.
- (18) Marques, S. M.; Nuti, E.; Rossello, A.; Supuran, C. T.; Tuccinardi, T.; Martinelli, A.; Santos, M. A. Dual inhibitors of matrix metalloproteinases and carbonic anhydrases: iminodiacetyl-based hydroxamate–benzenesulfonamide conjugates. *J. Med. Chem.* **2008**, *51*, 7968–7979.
- (19) Chaves, S.; Marques, S.; Santos, M. A. Iminodiacetyl-hydroxamate derivatives as metalloproteinase inhibitors: equilibrium complexation studies with Cu(II), Zn(II) and Ni(II). *J. Inorg. Biochem.* **2003**, *97*, 345–353.
- (20) Nuti, E.; Panelli, L.; Casalini, F.; Avramova, S. I.; Orlandini, E.; Santamaria, S.; Nencetti, S.; Tuccinardi, T.; Martinelli, A.; Cercignani, G.; D'Amelio, N.; Maiocchi, A.; Uggeri, F.; Rossello, A. Design, synthesis, biological evaluation, and NMR studies of a new series of arylsulfones as selective and potent matrix metalloproteinase-12 inhibitors. *J. Med. Chem.* **2009**, *52*, 6347–6361.
- (21) Nuti, E.; Casalini, F.; Avramova, S. I.; Santamaria, S.; Cercignani, G.; Marinelli, L.; La Pietra, V.; Novellino, E.; Orlandini, E.; Nencetti, S.; Tuccinardi, T.; Martinelli, A.; Lim, N. H.; Visse, R.; Nagase, H.; Rossello, A. *N*-*O*-Isopropyl sulfonamido-based hydroxamates: design, synthesis and biological evaluation of selective matrix metalloproteinase-13 inhibitors as potential therapeutic agents for osteoarthritis. *J. Med. Chem.* **2009**, *52*, 4757–4773.
- (22) Topf, M.; Varnai, P.; Richards, W. G. Ab initio QM/MM dynamics simulation of the tetrahedral intermediate of serine proteases: insights into the active site hydrogen-bonding network. *J. Am. Chem. Soc.* **2002**, *124*, 14780–14788.
- (23) Yonezawa, Y.; Nakata, K.; Sakakura, K.; Takada, T.; Nakamura, H. Intra- and Intermolecular Interaction Inducing Pyramidalization on Both Sides of a Proline Dipeptide during Isomerization: An ab Initio QM/MM Molecular Dynamics Simulation Study in Explicit Water. *J. Am. Chem. Soc.* **2009**, *131*, 4535–4540.
- (24) Case, D. A.; Darden, T. A.; Cheatham, T. E., III; Simmerling, C. L.; Wang, J.; Duke, R. E.; Luo, R.; Crowley, M.; Walker, R. C.; Zhang, W.; Merz, K. M.; Wang, B.; Hayik, S.; Roitberg, A.; Seabra, G.; Kolossváry, I.; Wong, K. F.; Paesani, F.; Vanicek, J.; Wu, X.; Brozell, S. R.; Steinbrecher, T.; Gohlke, H.; Yang, L.; Tan, C.; Mongan, J.; Hornak, V.; Cui, G.; Mathews, D. H.; Seetin, M. G.; Sagui, C.; Babin, V.; Kollman, P. A. AMBER, version 10; University of California: San Francisco, CA, 2008.
- (25) Seifert, G.; Porezag, D.; Frauenheim, T. Calculations of molecules, clusters, and solids with a simplified LCAO-DFT-LDA scheme. *Int. J. Quantum Chem.* **1996**, *58*, 185–192.
- (26) Tuccinardi, T.; Martinelli, A.; Nuti, E.; Carelli, P.; Balzano, F.; Uccello-Barretta, G.; Murphy, G.; Rossello, A. Amber force field implementation, molecular modelling study, synthesis and MMP-1/MMP-2 inhibition profile of (*R*)- and (*S*)-*N*-hydroxy-2-(*N*-isopropoxybiphenyl-4-ylsulfonamido)-3-methylbutanamides. *Bioorg. Med. Chem.* **2006**, *14*, 4260–4276.

- (27) Toba, S.; Damodaran, K. V.; Merz, K. M. Jr. Binding preferences of hydroxamate inhibitors of the matrix metalloproteinase human fibroblast collagenase. *J. Med. Chem.* **1999**, *42*, 1225–1234.
- (28) Donini, O. A.; Kollman, P. A. Calculation and prediction of binding free energies for the matrix metalloproteinases. *J. Med. Chem.* **2000**, *43*, 4180–4188.
- (29) Lovejoy, B.; Welch, A. R.; Carr, S.; Luong, C.; Broka, C.; Hendricks, R. T.; Campbell, J. A.; Walker, K. A.; Martin, R.; Van Wart, H.; Browner, M. F. Crystal structures of MMP-1 and -13 reveal the structural basis for selectivity of collagenase inhibitors. *Nature Struct. Biol.* **1999**, *6*, 217–221.
- (30) Blagg, J. A.; Noe, M. C.; Wolf-Gouveia, L. A.; Reiter, L. A.; Laird, E. R.; Chang, S. P.; Danley, D. E.; Downs, J. T.; Elliott, N. C.; Eskra, J. D.; Griffiths, R. J.; Hardink, J. R.; Haugeto, A. I.; Jones, C. S.; Liras, J. L.; Lopresti-Morrow, L. L.; Mitchell, P. G.; Pandit, J.; Robinson, R. P.; Subramanyam, C.; Vaughn-Bowser, M. L.; Yocum, S. A. Potent pyrimidinetrione-based inhibitors of MMP-13 with enhanced selectivity over MMP-14. *Bioorg. Med. Chem. Lett.* **2005**, *15*, 1807–1810.
- (31) Nuti, E.; Tuccinardi, T.; Rossello, A. Matrix metalloproteinase inhibitors: new challenges in the era of post broad-spectrum inhibitors. *Curr. Pharm. Des.* **2007**, *13*, 2087–2100.
- (32) Santos, M. A.; Marques, S. M.; Tuccinardi, T.; Carelli, P.; Panelli, L.; Rossello, A. Design, synthesis and molecular modeling study of iminodiacetyl monohydroxamic acid derivatives as MMP inhibitors. *Bioorg. Med. Chem.* **2006**, *14*, 7539–7550.
- (33) Breyholz, H. J.; Wagner, S.; Faust, A.; Riemann, B.; Holtke, C.; Hermann, S.; Schober, O.; Schafers, M.; Kopka, K. Radiofluorinated pyrimidine-2,4,6-triones as molecular probes for noninvasive MMP-targeted imaging. *ChemMedChem* **2010**, *5*, 777–789.
- (34) Yu, W.; Guo, Z.; Orth, P.; Madison, V.; Chen, L.; Dai, C.; Feltz, R. J.; Girijavallabhan, V. M.; Kim, S. H.; Kozlowski, J. A.; Lavey, B. J.; Li, D.; Lundell, D.; Niu, X.; Piwinski, J. J.; Popovici-Muller, J.; Rizvi, R.; Rosner, K. E.; Shankar, B. B.; Shih, N. Y.; Siddiqui, M. A.; Sun, J.; Tong, L.; Umland, S.; Wong, M. K.; Yang, D. Y.; Zhou, G. Discovery and SAR of hydantoin TACE inhibitors. *Bioorg. Med. Chem. Lett.* **2010**, *20*, 1877–1880.
- (35) Yu, W.; Tong, L.; Kim, S. H.; Wong, M. K.; Chen, L.; Yang, D. Y.; Shankar, B. B.; Lavey, B. J.; Zhou, G.; Kosinski, A.; Rizvi, R.; Li, D.; Feltz, R. J.; Piwinski, J. J.; Rosner, K. E.; Shih, N. Y.; Siddiqui, M. A.; Guo, Z.; Orth, P.; Shah, H.; Sun, J.; Umland, S.; Lundell, D. J.; Niu, X.; Kozlowski, J. A. Biaryl substituted hydantoin compounds as TACE inhibitors. *Bioorg. Med. Chem. Lett.* **2010**, *20*, 5286–5289.
- (36) Pikul, S.; Dunham, K. M.; Almstead, N. G.; De, B.; Natchus, M. G.; Taiwo, Y. O.; Williams, L. E.; Hynd, B. A.; Hsieh, L. C.; Janusz, M. J.; Gu, F.; Mieling, G. E. Heterocycle-based MMP inhibitors with P2' substituents. *Bioorg. Med. Chem. Lett.* **2001**, *11*, 1009–1013.
- (37) Armarego, W. L. F.; Perrin, D. D., *Purification of Laboratory Chemicals*, 4th ed.; Butterworth-Heinemann: Oxford, 1999.
- (38) Bruker AXS: SAINT+, release 6.22; Bruker Analytical Systems: Madison, WI, 2005.
- (39) Altomare, A.; Burla, M. C.; Camalli, M.; Cascarano, G. L.; Giacovazzo, C.; Guagliardi, A.; Moliterni, A. G. G.; Polidori, G.; Spagna, R. SIR97: a new tool for crystal structure determination and refinement. *J. Appl. Crystallogr.* **1999**, *32*, 115–119.
- (40) Sheldrick, G. M. A short history of SHELX. *Acta Crystallogr., Sect. A: Found. Crystallogr.* **2008**, *64* (Pt 1), 112–122.
- (41) Barnes, C. L. ORTEP-3 for Windows—a version of ORTEP-III with a Graphical User Interface (GUI). *J. Appl. Crystallogr.* **1997**, *30*, 568–568.
- (42) Macrae, C. F.; Bruno, I. J.; Chisholm, J. A.; Edgington, P. R.; McCabe, P.; Pidcock, E.; Rodriguez-Monge, L.; Taylor, R.; van de Streek, J.; Wood, P. A. Mercury CSD 2.0—new features for the visualization and investigation of crystal structures. *J. Appl. Crystallogr.* **2008**, *41*, 466–470.
- (43) Knight, C. G.; Willenbrock, F.; Murphy, G. A novel coumarin-labelled peptide for sensitive continuous assays of the matrix metalloproteinases. *FEBS Lett.* **1992**, *296*, 263–266.
- (44) Voigt, J. H.; Elkin, C.; Madison, V. S.; Duca, J. S. Cross-docking of inhibitors into CDK2 structures. 2. *J. Chem. Inf. Model.* **2008**, *48*, 669–678.
- (45) Gleeson, M. P.; Gleeson, D. QM/MM as a tool in fragment based drug discovery. A cross-docking, rescoring study of kinase inhibitors. *J. Chem. Inf. Model.* **2009**, *49*, 1437–1448.
- (46) Maestro, version 9.0; Schrödinger Inc.: Portland, OR, 2009.
- (47) MacroModel, version 9.7; Schrödinger Inc.: Portland, OR, 2009.
- (48) Berman, H. M.; Westbrook, J.; Feng, Z.; Gilliland, G.; Bhat, T. N.; Weissig, H.; Shindyalov, I. N.; Bourne, P. E. The Protein Data Bank. *Nucleic Acids Res.* **2000**, *28*, 235–242.
- (49) Verdonk, M. L.; Cole, J. C.; Hartshorn, M. J.; Murray, C. W.; Taylor, R. D. Improved protein–ligand docking using GOLD. *Proteins* **2003**, *52*, 609–623.
- (50) Essmann, U.; Perera, L.; Berkowitz, M. L.; Darden, T.; Lee, H.; Pedersen, L. G. A smooth particle mesh Ewald method. *J. Chem. Phys.* **1995**, *103*, 8577–8593.
- (51) Frisch, M. J.; Trucks, G. W.; Schlegel, H. B.; Scuseria, G. E.; Robb, M. A.; Cheeseman, J. R.; Montgomery, J., J. A.; Vreven, T.; Kudin, K. N.; Burant, J. C.; Millam, J. M.; Iyengar, S. S.; Tomasi, J.; Barone, V.; Mennucci, B.; Cossi, M.; Scalmani, G.; Rega, N.; Petersson, G. A.; Nakatsuji, H.; Hada, M.; Ehara, M.; Toyota, K.; Fukuda, R.; Hasegawa, J.; Ishida, M.; Nakajima, T.; Honda, Y.; Kitao, O.; Nakai, H.; Klene, M.; Li, X.; Knox, J. E.; Hratchian, H. P.; Cross, J. B.; Bakken, V.; Adamo, C.; Jaramillo, J.; Gomperts, R.; Stratmann, R. E.; Yazyev, O.; Austin, A. J.; Cammi, R.; Pomelli, C.; Ochterski, J. W.; Ayala, P. Y.; Morokuma, K.; Voth, G. A.; Salvador, P.; Dannenberg, J. J.; Zakrzewski, V. G.; Dapprich, S.; Daniels, A. D.; Strain, M. C.; Farkas, O.; Malick, D. K.; Rabuck, A. D.; Raghavachari, K.; Foresman, J. B.; Ortiz, J. V.; Cui, Q.; Baboul, A. G.; Clifford, S.; Cioslowski, J.; Stefanov, B. B.; Liu, G.; Liashenko, A.; Piskorz, P.; Komaromi, I.; Martin, R. L.; Fox, D. J.; Keith, T.; Al-Laham, M. A.; Peng, C. Y.; Nanayakkara, A.; Challacombe, M.; Gill, P. M. W.; Johnson, B.; Chen, W.; Wong, M. W.; Gonzalez, C.; Pople, J. A. *Gaussian 03*, revision C.02; Gaussian, Inc.: Wallingford, CT, 2004.